ACS OMEGA

http://pubs.acs.org/journal/acsodf

Article

Enrichment of Oxygen-Containing Low-Concentration Coalbed Methane with CMS-3KT as the Adsorbent

Jie Zhang, Hong Liu,* Fubao Zhou,* Xingcheng Li, Kangwei Wei, and Jiaojiao Song

Cite This: *ACS Omega* 2021, 6, 6914−6923

Read Online

ACCESS | Metrics & More | Article Recommendations | Supporting Information

ABSTRACT: A type of carbon molecular sieve (CMS-3KT) was used as the adsorbent for the CH_4 enrichment of a methane/oxygen/nitrogen ($CH_4/O_2/N_2$) mixture using micro-positive pressure vacuum pressure swing adsorption (~120 kPa). The adsorption isotherms of individual CH_4, O_2, and N_2 on CMS-3KT were studied and fitted. The results indicated the important influence of the adsorbent surface heterogeneity on the adsorption equilibrium process. In addition, the interaction of adsorbent−adsorbate in this process was studied from the measured adsorption heat. The adsorption uptake curves were fitted linearly with a classical micropore model for evaluating the kinetics-based separation possibility of $CH_4/O_2/N_2$, and the corresponding diffusion time constants of CH_4, O_2, and N_2 were calculated. Based on the results of adsorption equilibrium and kinetics, breakthrough experiments were employed to explore the upper limit value of methane concentration in feed gas such that methane can be enriched feasibly but difficultly. The breakthrough experiments were performed on the $CH_4/O_2/N_2$ mixture with CH_4 concentration ranging from 1 to 30%. Regarding industrial application, the O_2 removal and CH_4 enrichment performance of ultra-low-concentration methane (CH_4 < 5%) were evaluated according to the results of the breakthrough experiment. The results indicated that the proposed method was promising for enriching O_2-containing ultra-low-concentration CBM.

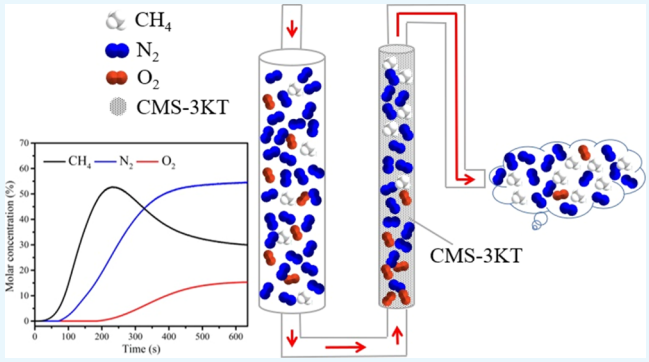

1. INTRODUCTION

Coalbed methane (CBM) is one of the clean energies and its recoverable amount is considerable, being ~42 Tm^3 globally.[1] In China, ~3.7 Tm^3 CBM is buried above 2000 m,[2] and most of the CBM extracted from coal seam is discharged directly into the atmosphere, especially for low-concentration methane (<30%). As a result, China's CBM emissions account for one-third[3] of global emissions and constitute a huge waste of natural gas resources. This amount of methane (CH_4) induces a large greenhouse effect because the greenhouse effect of CH_4 is 23 times that of CO_2.[4] Therefore, the recycling and utilization of low-concentration CBM is important from both economic and environmental viewpoints.[5−8]

CBM contains mainly methane, oxygen (O_2), nitrogen (N_2), and a small amount of CO_2 and H_2O. In order to meet the quality requirements stipulated for the use of CBM, many methods have been developed for CH_4 enrichment. The pressure swing adsorption (PSA)[9,10] process has been extensively used and is regarded as the most promising technology for CH_4 enrichment of CBM. The preference for this technology results from its simpler operation and less energy consumption compared with other methods such as cryogenic distillation,[11] membrane separation,[12] and hydrate formation.[13]

Saleman et al.[14] enriched CH_4 from 10.4 to 40.2% in a CH_4/N_2 binary mixture using dual-reflux PSA, with methane recovery of 71%. Qu et al.[15] reported an increase (from 21.4% to nearly 47%) in the concentration of CH_4, and the recovery of methane was around 75%. Zhang et al.[16] used PSA to separate 27%/73% CH_4/N_2, and CH_4 was purified to 57.2%, with methane recovery of around 91%. Vacuum pressure swing adsorption (VPSA) with activated carbon was used by Gu et al.[17] to separate binary mixtures of 30%/70% CH_4/N_2, and a CH_4 enrichment of 66.6% was achieved. However, O_2 was neglected in the above studies.

Oxygen is a major component of CBM, and its presence increases the risk of explosion in the transportation and utilization of low-concentration CBM. Thus, O_2 removal is especially important for the enrichment and utilization of O_2-containing low-concentration CBM. Carbon molecular sieve (CMS) is a kind of good non-polar carbon material and is

Received: December 17, 2020
Accepted: February 12, 2021
Published: March 5, 2021

currently a preferred PSA adsorbent for removing O_2 from mixture gases due to its considerable micropore volume and pore size distribution. The feasibility of O_2 removal and CH_4 enrichment of O_2-containing CBM with CMS has been demonstrated in some studies.

Bae et al.[18] determined (from a kinetics viewpoint) the probability of separation for CH_4, N_2, and O_2 on CMS-3TA by calculating the diffusion time constants of these gases. In another work,[19] different models were used to analyze the adsorption rate of each gas on CMS-3TA, as the rates can contribute to the separation of the gases at different pressures. Liu et al.[20,21] used proportion PSA with activated carbon (AC) and CMS to separate a ternary mixture of 20%/17%/63% $CH_4/O_2/N_2$. Although CH_4 was purified from 20% to more than 50% by this method, the adsorbed column was impractical for the real separation process. Olajossy et al.[22,23] purified CH_4 to 96% from a ternary mixture of 55%/8%/37% $CH_4/O_2/N_2$ with the recovery of methane about 86% using PSA at a pressure of 300 kPa. Zhou et al.[24] achieved a CH_4 concentration of 50.4% from a ternary mixture of 25%/7%/65% $CH_4/O_2/N_2$ at a pressure of 300 kPa, and the methane recovery was nearly 86.3%. Yang et al.[25] enriched CH_4 to more than 90% from a ternary mixture of 30%/14.7%/55.3% $CH_4/O_2/N_2$ (methane recovery around 54%) using CMS at a pressure of 250 kPa, and the kinetics-based separation mechanism was investigated.

The above studies have (to some extent) analyzed the equilibrium performance and kinetic behavior associated with the separation of $CH_4/O_2/N_2$ mixture on CMSs. However, published reports on the enrichment of O_2-containing CBM with CH_4 concentrations of <5% are rare. The pressure employed in the process of CH_4 enrichment was >120 kPa, which differs from the actual outlet pressure of CBM in coal mines. The costs and explosion risks increase in the pressurization process. In addition, the participation of helium (He) in the CH_4 enrichment processes can only be experimentally studied but cannot applied in practical working condition.

In this work, the equilibrium performance and kinetic behavior of CH_4, O_2, and N_2 on CMS-3KT were investigated from the adsorption capacity of individual gases. The adsorbate−sorbent interactions were evaluated based on the adsorption heat. Then, the breakthrough experiment for $CH_4/O_2/N_2$ mixture with different CH_4 concentrations was implemented to verify the results of adsorption equilibrium and kinetics. In addition, the upper limit value of methane concentration in feed gas that methane can be enriched feasibly but difficultly would be derived from the breakthrough experiment. Finally, the removal of oxygen and enrichment of methane from the $CH_4/O_2/N_2$ mixture were studied considering practical application, with the method of micro-positive pressure VPSA (~120 kPa). The above results could provide a valuable direction for oxygen removal and methane purification of CBM.

2. RESULTS AND DISCUSSION

2.1. Characterization. The micropore volume and specific surface area of CMS-3KT were 0.24 cm^3/g and 407.8 m^2/g, respectively. Figure 1 shows highly developed microporosity with the pore size ranging from 0.37 to 0.91 nm, which was comparable to the kinetic diameter of CH_4, O_2, and N_2. Hence, CH_4, O_2, and N_2 could all be well adsorbed.

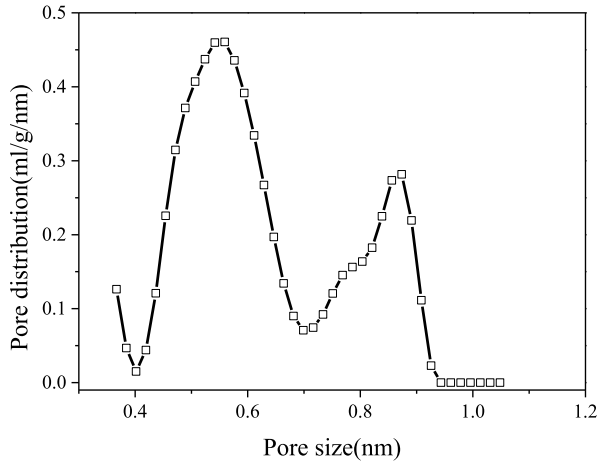

Figure 1. Micropore size distribution of CMS-3KT.

2.2. Adsorption Equilibrium. *2.2.1. Adsorption Isotherms.* The adsorption isotherms of CH_4, O_2, and N_2 associated with a pressure of 0−0.6 MPa and a temperature of 308 K are presented in Figure 2 (313 and 318 K in Figure S1). These isotherms were designated as type I based on the IUPAC classification.[26] The adsorption amounts increase with decreasing temperature, consistent with the exothermic process of adsorption.[27] The main reason is that the gas molecules have more energy to desorb from the adsorbent in higher temperature. The higher adsorption amount of CH_4 (compared with those of O_2 and N_2) was attributed to its higher polarizability; that is, the adsorption of these gases on CMS-3KT resulted mainly from dispersion interactions.[28] The adsorption amounts of CH_4, O_2, and N_2 (1.2−1.6, 0.85−0.97, and 0.71−0.78 mmol/g, respectively) were all considerable. This may have resulted from the vast surface area (407.8 m^2/g) and the adaptive micropore size distribution (0.37−0.91 nm) of CMS-3KT. The reference data[18,19,25,29−34] of CMS are shown in Table S1. Considering the differences in the surface area and pore structure, the experimental results in this study were reasonable.

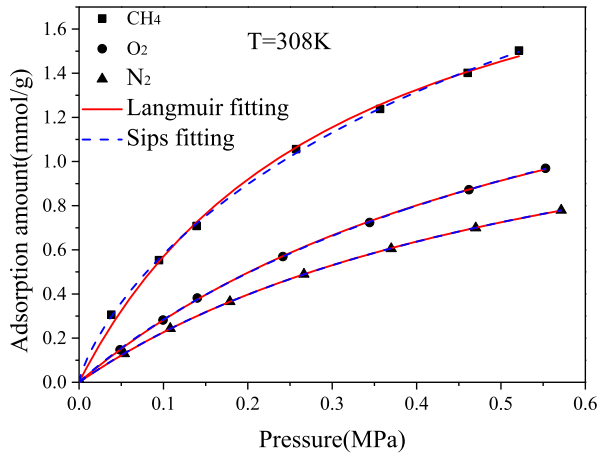

Figure 2. Adsorption isotherms of CH_4, O_2, and N_2 at 308 K.

The experimental data were fitted by Langmuir and Sips models, as shown in Figure 2. For the entire adsorption process, the Sips models predicted the adsorption isotherms slightly better than the Langmuir model. The fitting parameters

https://dx.doi.org/10.1021/acsomega.0c06148
ACS Omega 2021, 6, 6914−6923

Table 1. Parameters Calculated from Langmuir and Sips Models Fitting the Adsorption Isotherms

gas	CH_4			O_2			N_2		
temperature (K)	308	313	318	308	313	318	308	313	318
				Langmuir					
q_m (mmol/g)	2.37	1.97	1.94	2.21	2.17	2.07	1.61	1.59	1.58
b (1/MPa)	3.24	3.16	2.16	1.58	1.28	1.16	1.64	1.53	1.46
MAPE (%)	3.50	3.78	4.11	0.58	1.74	4.58	0.30	0.36	0.23
				Sips					
q_m (mmol/g)	3.73	3.62	3.45	2.25	1.90	1.72	1.63	1.61	1.60
b (1/MPa)	1.26	1.15	1.07	1.74	1.67	1.35	1.59	1.50	1.43
n	1.37	1.35	1.33	1.03	0.94	0.91	1.01	1.01	1.01
MAPE (%)	1.22	2.04	3.83	0.76	1.05	3.54	0.36	0.38	0.25

and MAPEs of the two models are shown in Table 1. A notable decline can be observed in the value of b with the rise of temperature. The MAPEs of CH_4 fitted by the Langmuir and Sips models were 3.50 and 1.22%, respectively. In addition, the q_m value for methane calculated from the Sips model was slightly bigger, might be because the value of $n(CH_4)$ was larger than 1. Thus, the non-homogeneity of the adsorbent surface affected the adsorption equilibrium process to some degree.

2.2.2. Adsorption Heat. The adsorption heat flow (see Figure 3) is measured using a C80 micro-calorimeter. The steep increase in the heat flow in the initial stage demonstrates that the vertical interaction occurred first at low surface loading and led to high adsorption heat. Moreover, the slow reduction was attributed to the lateral interaction at high surface loading. The variation in the adsorption heat with the surface loading resulted possibly from the fact that the lateral interaction occurred between the adsorbed gas molecules.[19,35,36]

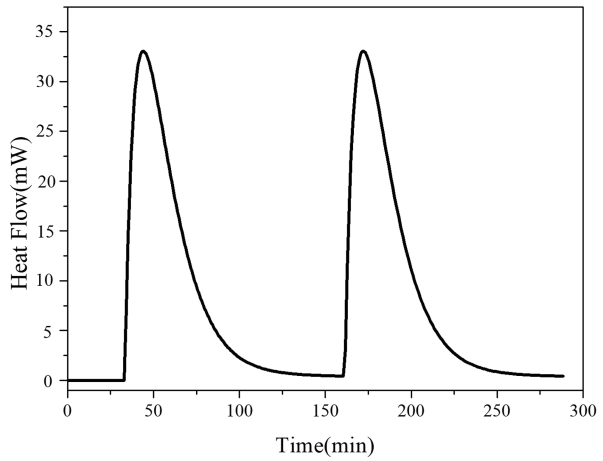

Figure 3. Adsorption heat flow measured by a C80 micro-calorimeter (e.g., N_2 is taken).

The integral heats of CH_4, O_2, and N_2 at different temperatures (Figure S2) are measured using a micro-calorimeter, and the corresponding adsorption isosteric heats are calculated, as shown in Figure 4. The differences among the above results were modest, because the interactions of CH_4, O_2, and N_2 molecules and the CMS-3KT surface resulted mainly from the inductive force and dispersion force, which are both independent of temperature. Isosteric heats of CH_4, O_2, and N_2 were ~20.6, 18.1, and 19.1 kJ/mol, respectively, in this work. The theoretical adsorption isosteric heats reported in the literature varied widely. For example, values of 18.0−39.0 kJ/mol have been reported for CH_4.[37−39] The adsorption heats of CH_4, O_2, and N_2 measured in this work were comparable to the theoretical values.[25,32,39−41]

The adsorption capacity of CH_4 on CMS-3KT was only approximately twice that of O_2 and N_2, and hence, easy removal of oxygen and separation of CH_4 from the mixture of $CH_4/O_2/N_2$ via adsorption equilibrium was impossible. Thus, another critical factor for adsorption separation, adsorption kinetics, was investigated.

2.3. Adsorption Kinetics. Figure 5 shows the adsorption uptake curves of the individual O_2, N_2, and CH_4 gases on CMS-3KT under 120 kPa. The adsorption rate of CH_4 was considerably lower than that of N_2 and O_2. Equilibration of O_2 and N_2 occurs in ~25 s and 10 min, respectively. However, more than 12 h was needed for equilibration of CH_4. The results indicated that the gases may be written in the descending order of adsorption rate on CMS-3KT, that is,

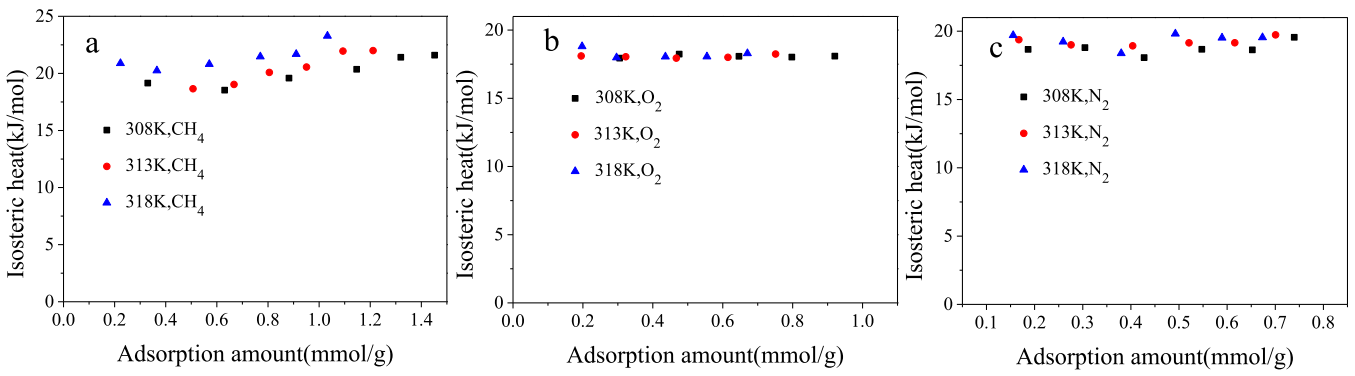

Figure 4. Isosteric heats of adsorption for CH_4 (a), O_2 (b), and N_2 (c) at 308, 313, and 318 K.

https://dx.doi.org/10.1021/acsomega.0c06148
ACS Omega 2021, 6, 6914−6923

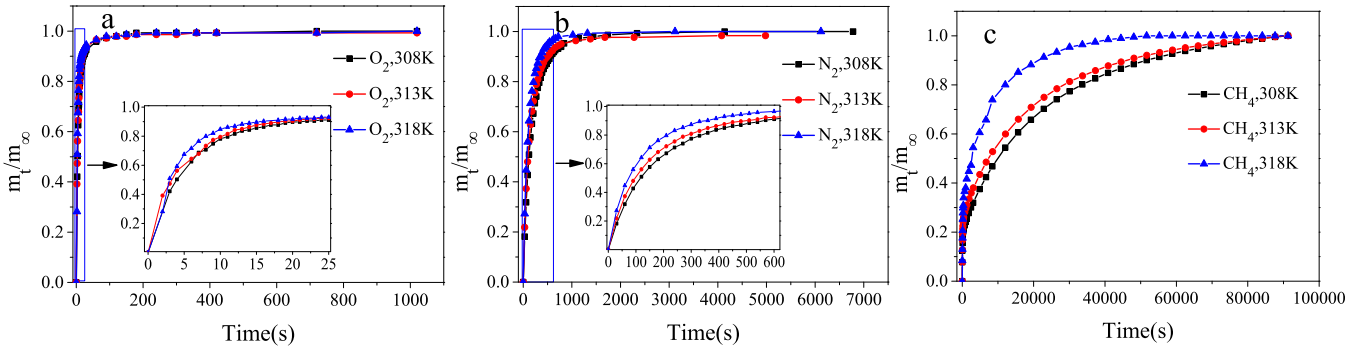

Figure 5. Adsorption uptake curves of O_2 (a), N_2 (b), and CH_4 (c) on CMS-3KT at 120 kPa in 308, 313, and 318 K, respectively.

Table 2. Diffusion Time Constants of CH_4, O_2, and N_2 in 308, 313, and 318 K

temperature (K)	$D_{e,O_2}/r_c^2$ (s^{-1}) $\times 10^{-3}$	$D_{e,N_2}/r_c^2$ (s^{-1}) $\times 10^{-4}$	$D_{e,CH_4}/r_c^2$(s^{-1}) $\times 10^{-6}$	$D_{e,O_2}/D_{e,CH_4}$	$D_{e,N_2}/D_{e,CH_4}$
308	0.86	3.39	3.83	2247.06	88.35
313	1.02	3.69	4.11	2484.07	89.87
318	1.11	5.23	8.41	1322.04	62.21

O_2 > N_2 > CH_4. Each rate increases slightly with increasing temperature. CH_4, with a substantially lower adsorption rate than the other gases, could be easily separated from the mixture of $CH_4/O_2/N_2$. The adsorption rate of a specific gas on CMS-3KT was strongly correlated with the ratio of the gas kinetic diameter to the pore size of the adsorbent. In this study, the micropore size of CMS-3KT ranged from 0.37 to 0.91 nm. The kinetic diameters of O_2, N_2, and CH_4 were 0.346, 0.364, and 0.376 nm, respectively,[40,41] which were close to the pore size of CMS-3KT. In addition, the critical diameters of N_2 and O_2 with linear molecular structures were 4.0 × 3.0 and 3.9 × 2.8 Å, respectively, while a diameter of 4.4 Å was obtained for CH_4 with a tetrahedron molecular structure.[28] Therefore, compared with CH_4, O_2 and N_2 could occupy the pores of CMS-3KT faster with the CMS-3KT internal surface. The possible reason was that the interaction and resistance between gas and CMS-3KT occurs with the increase in molecular size. Furthermore, a spin−spin interaction occurred between O_2 molecules, and a quadrupole moment was present in N_2.[42,43] However, these interactions and moments are absent from CH_4. Therefore, the slow adsorption rate of CH_4 was also explained by its stable electronic structures.

The diffusion time constant (D_e/r^2) is an essential parameter for quantifying the adsorption rate and evaluating the CH_4 enrichment performance, which varies with the temperature. Therefore, in this work, the kinetic data of O_2, N_2, and CH_4 at 308, 313, and 318 K were fitted by a classical micropore diffusion model (see Figure S3). The D_e/r^2 value (Table 2) was simultaneously calculated. R^2 values of 0.99 indicate that the model predicts the kinetic process accurately. The gases may be written in descending order of D_e/r^2, where O_2 > N_2 > CH_4. Each D_e/r^2 value increased slightly with increasing temperature. These results are consistent with those of previous studies.[25,31] The diffusion ratio of each gas pair was calculated, and the high values of $D_{e,O_2/CH_4}$ (>1000) and $D_{e,N_2/CH_4}$ (>60) demonstrated that (in theory) O_2 removal and CH_4 enrichment of CBM could be performed without temperature restrictions (308−318 K).

2.4. Evaluation of Separation Performance. The adsorption selectivity of $CH_4/O_2/N_2$ on CMS-3KT was assessed via breakthrough experiments. The breakthrough curves for the $CH_4/O_2/N_2$ mixture with CH_4 concentrations of 1, 3, 5, 10, 15, and 30% on CMS-3KT were measured at an inlet flow velocity of 80 mL/min, as shown in Figure 6. The breakthrough times were obtained accordingly and listed in Table 3, which corresponds to the point on the breakthrough curve when the outflow concentration of a specific gas reaches 5% of its initial concentration. In all cases, the breakthrough time of O_2 was longer than those of N_2 and CH_4, owing to the greater adsorption rate of O_2, as shown in the uptake curve. This is consistent with the fact that the diffusion time constant of O_2 is ∼2248 and 30 times those of CH_4 and N_2, respectively. The extremely long penetration time of O_2 demonstrated that CH_4 was enriched effectively from CBM and revealed the considerable benefit of micro-positive pressure VPSA in removing O_2 from O_2-containing CBM. For example, compared with that achieved via combustion[44] and catalysis[45] methods, higher safety and CH_4 recovery were realized for the O_2 removal method presented in this work.

In addition, the integral difference in Figure 6 between CH_4 and N_2 decreases significantly with the decrease of CH_4 concentration, indicating more difficulty to separate CH_4 and N_2. This was attributed to the fact that, with the decrease of CH_4 concentration in feed gas, the adsorption amounts of CH_4 exceeded the supplement. However, the breakthrough time of N_2 was obviously larger than that of CH_4 even when the concentration of CH_4 is equal to or lower than 5% (Table 3). Thus, product gas with higher concentration CH_4 could be collected before N_2 penetration. Therefore, the upper limit value of methane concentration in feed gas that methane can be enriched feasibly but difficultly could be regarded as 5%, and the following enrichment experiments of methane would be based on it. The separation performance for the mixture of $CH_4/O_2/N_2$ should be determined without the use of He. The replacement of He with pure CH_4 in the pressurization process was considered in a previous study.[25] However, the hypothesis was unreasonable to some extent because the diffusion rates of O_2 and N_2 were both substantially larger than that of CH_4.

2.5. Evaluation of Enrichment Performance in Micro-positive Pressure VPSA. *2.5.1. Influence of Gas Flow Velocity on CH_4 Enrichment.* The enrichment of CH_4 from the prepared ultra-low-concentration CBM was performed

https://dx.doi.org/10.1021/acsomega.0c06148
ACS Omega 2021, 6, 6914−6923

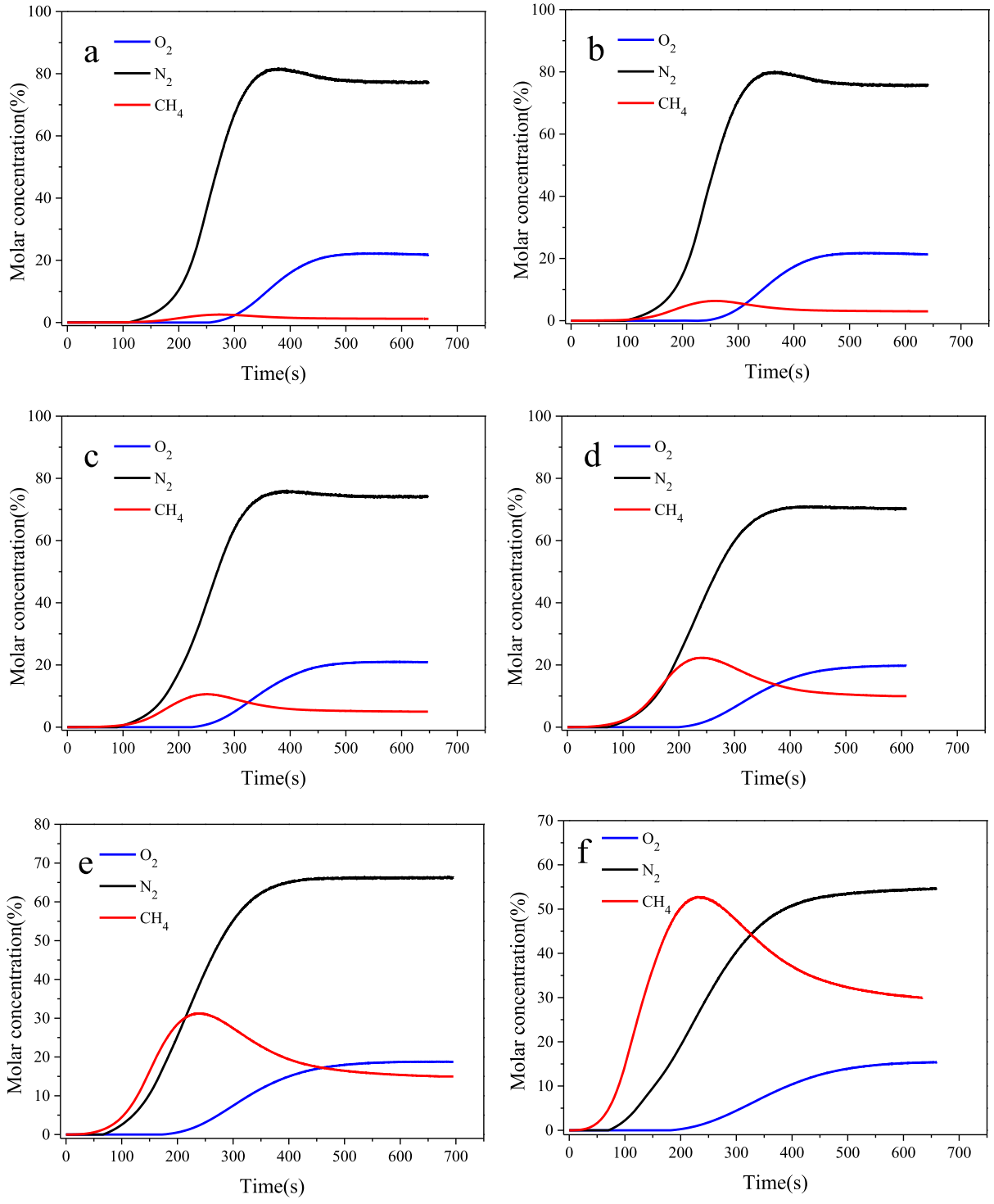

Figure 6. Breakthrough curves of $CH_4/O_2/N_2$ with CH_4 concentrations of 1 (a), 3 (b), 5 (c), 10 (d), 15 (e), and 30% (f).

experimentally without the participation of He. A gasholder is installed before the adsorption bed to provide enough pressure for the instantaneous penetration of the gas components. The real-time concentrations of CH_4, O_2, and N_2 with initial CH_4 concentrations of 1, 3, and 5% are shown in Figure 7. The maximum concentration of CH_4 declines and the minimum concentration of O_2 increases as the inlet flow velocity increased from 200 mL/min to 600 mL/min. On the one hand, higher flow velocity resulted in weaker interaction force between O_2 and adsorbent. On the other hand, the mass transfer resistance became important and had a compensation effect with the increase of flow velocity, leading to smaller superiority of CH_4 in the product. Considering an inlet flow velocity of 200 mL/min and initial CH_4 concentrations of 1, 3, and 5%, the concentrations of CH_4 are enriched to maximum levels of 4.5, 8.8, and 13.5%, and the concentrations of O_2 are reduced to minimum levels of 3.8, 3.0, and 2.5%, respectively (see Figure 7a). This may have resulted from the fact that the amount of methane in the gasholder was sufficient for achieving the adsorption selectivity of the adsorbent.

https://dx.doi.org/10.1021/acsomega.0c06148
ACS Omega 2021, 6, 6914−6923

Table 3. Breakthrough Time for CH_4, O_2, and N_2 with Different Concentrations of CH_4 in Feed Gas

the composition of feed gas			breakthrough time (s)		
CH_4 (%)	N_2 (%)	O_2 (%)	CH_4	N_2	O_2
1	78.2	20.8	94.1	164.5	283.4
3	76.6	20.4	82.3	150.1	267.3
5	75.0	20.0	74.0	139.4	254.3
10	71.1	18.9	61.4	118.5	233.1
15	67.2	17.8	55.3	108.5	213.0
30	55.3	14.7	48.5	104.5	221.6

In fact, the average concentration was more significant than the transient concentration for CBM enrichment. A certain period was defined as the effective time (T), in which the concentration of O_2 is less than 5%. Simultaneously, the concentration of methane was large in this period, indicative of the appropriate time period for collecting the product gas. There was an increase in effective time with the rise of CH_4 concentration in feed gas ($T1 < T2 < T3$), consistent with the result in breakthrough experiment, that is, the integral difference between the concentrations of CH_4 and N_2 increased significantly with rising CH_4 concentration in feed gas. A decline was observed in effective time with the increase in flow velocity, which was ascribed to the faster saturation of the adsorption bed. Hence, the best separation was observed at an inlet flow velocity of 200 mL/min, and the detailed enrichment performance is discussed in the following.

2.5.2. Oxygen Removal and Methane Enrichment Effect. CH_4 recovery is an essential criterion for evaluating the CBM enrichment performance. Hence, the CH_4 recoveries of product gas in different periods were investigated, and the average concentrations of O_2 and CH_4 (see Table 4) were measured simultaneously.

Considering the convenient and effective utilization of methane, the product gas was collected from 0 min. Although the high concentration of O_2 occurs in initiative moment, it has a slight effect in removing oxygen because of the slow flow velocity of outlet gas in this period. The optimal value was realized within 0−3 min at an acceptable concentration and recovery rate of methane. For example, the concentration of CH_4 was enriched to 12.3% with a recovery rate of 81.9% for 5% feed gas, and the concentration of O_2 was reduced to 3.23% simultaneously. The CH_4 concentrations of product gas were 2.82, 2.55, and 2.46 times that of the feed gas with methane concentrations of 1, 3, and 5%, respectively. This is consistent with the fact that the breakthrough time difference between CH_4 and N_2 occurs with the decline in CH_4 concentration of the feed gas during the breakthrough experiment. Therefore, the adsorption selectivity of the adsorbent decreased gradually before 3 min, and the number of O_2 and N_2 adsorption sites in the adsorbent was almost equal to the number of CH_4 sites after 3 min. The enrichment performance decreased with the saturation of the adsorption bed. Thus, the concentration and recovery of CH_4 should be considered reasonably in the collection of the product gas.

Table 4. Average O_2 and CH_4 Concentration and CH_4 Recovery Rate in the Product Collected from Different Periods at an Inlet Flow Velocity of 200 mL/min for the $CH_4/O_2/N_2$ Mixture

feed gas		product gas		
CH_4 (%)	period of time (min)	O_2 (%)	CH_4 (%)	recovery rate of CH_4 (%)
1	0−1	8.65	1.58	24.4
	0−2	7.70	2.78	47.7
	0−3	5.64	2.82	79.1
	0−4	6.72	2.28	86.6
	0−5	8.13	1.83	88.3
3	0−1	4.72	7.13	22.8
	0−2	3.41	7.14	54.9
	0−3	3.39	7.66	76.4
	0−4	4.29	6.16	83.1
	0−5	7.95	5.43	91.1
5	0−1	5.90	5.23	21.5
	0−2	5.37	8.98	40.8
	0−3	3.23	12.3	81.9
	0−4	4.90	10.5	89.4
	0−5	8.78	8.87	89.9

3. CONCLUSIONS

The considerable adsorption capacity of CH_4, O_2, and N_2 on CMS-3KT was attributed to the highly developed micropore structure of the adsorbent. The adsorbent−adsorbate interaction was induced mainly by an inductive force and dispersion force, with the occurrence of both vertical and lateral interactions. Moreover, the reversible adsorption process indicated that CH_4 enrichment was achieved via the adsorption method. The diffusion time constants of O_2 and N_2 were 2247 and 88 times, respectively, that of CH_4, demonstrating that kinetics-based separation of CH_4 from the $CH_4/O_2/N_2$

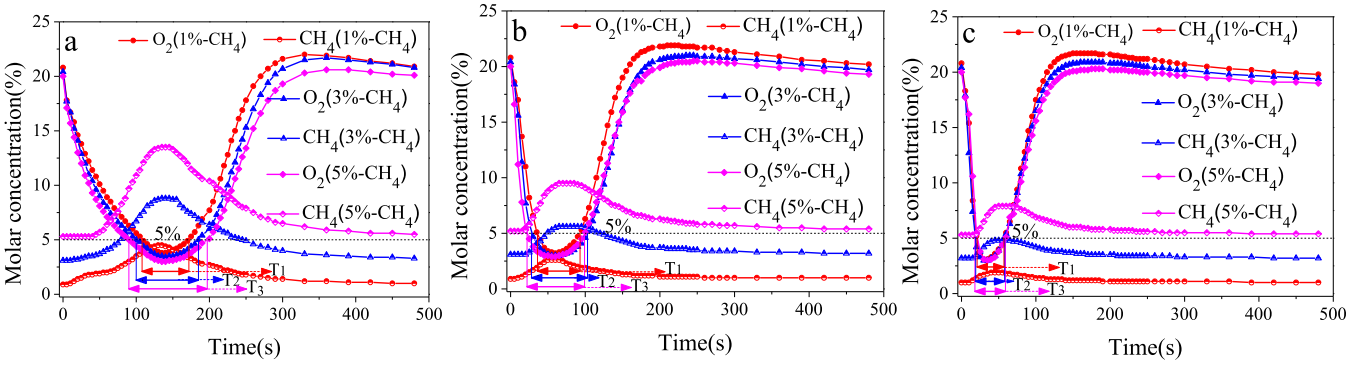

Figure 7. Real-time concentrations of O_2 and CH_4 over time at the inlet flow velocity of 200 (a), 400 (b), and 600 mL/min (c) with initial CH_4 concentrations of 1, 3, and 5%.

https://dx.doi.org/10.1021/acsomega.0c06148
ACS Omega 2021, 6, 6914−6923

mixture was possible. This was further confirmed by the breakthrough experimental results, where the breakthrough time of CH_4 was smaller than that of O_2 and N_2. Also, the upper limit value of methane concentration in feed gas such that methane can be enriched feasibly but difficultly is around 5%. Based on the above analysis, the enrichment performance of ultra-low-concentration methane (CH_4 < 5%) was evaluated. At a selected inlet flow velocity of 200 mL/min, the optimal enrichment performance was realized within a period of 0−3 min. The CH_4 concentration of the collected product gas was nearly 2.5 times that of the feed gas, with a recovery of ∼80%, and the O_2 concentrations were reduced to ∼3% simultaneously. The concentration and recovery of CH_4 should be balanced in practical application. Therefore, the proposed process had the prospect for removing oxygen and enriching methane from O_2-containing low-concentration CBM in industrial application.

4. EXPERIMENTAL MEASUREMENTS AND MATHEMATICAL MODELS

4.1. Experimental Measurements. *4.1.1. Materials.* Commercial CMS-3KT provided by Gongyi Tenglong Water Treatment Materials Co. Ltd. was selected as the adsorbent in this work. It was pre-activated at 673 K in N_2 flow for 4 h before use and the mass loss is around 5.45%. He (purity: 99.999%), CH_4 (purity: 99.999%), and air used in the experiments were supplied by Xuzhou Special Gas Plant.

4.1.2. Structural Characterization. The surface area and microporous structure of CMS-3KT were measured using an automated gas sorption analyzer (ASAP2460, Micromeritics Instruments, USA). The adsorption isotherm of CO_2 at 273 K was employed to obtain the surface area and micropore size distribution of the adsorbent using the density functional theory (DFT) method. In addition, the pore volume was calculated via the D−A model.[46]

4.1.3. Adsorption Equilibrium and Kinetics. The adsorption capacity and uptake curve of individual CH_4, O_2, and N_2 on CMS-3KT with different temperatures were measured by means of a volumetric method[47] using a self-built adsorption apparatus. CMS-3KT (4.6 g) was activated in advance and placed in the adsorption cell. He was used to check the gas tightness of the overall apparatus. The dead volume of the gas collector and adsorption cell was calculated from the He volume. Before measuring the adsorption isotherm, the system vacuum degree was maintained at approximately −0.1 MPa. The adsorption equilibrium point was determined after a constant pressure was maintained for at least 1 h. Furthermore, the adsorption heat was measured using a Tian-Calvet type C80 micro-calorimeter. By repeating this process, the equilibrium adsorption amounts at various pressures and corresponding adsorption heats were obtained. The details of the experiment are provided in our previous study.[48]

4.1.4. Separation Performance of the $CH_4/O_2/N_2$ Mixture. The breakthrough experiment on the $CH_4/O_2/N_2$ mixture with different CH_4 concentrations was performed using a multi-component adsorption breakthrough curve analyzer [Beishide Instrument Technology (Beijing) Co., Ltd.], as shown in Figure 8a. First, 60 g of CMS-3KT was placed in a packed column (length: 45 cm, diameter: 2 cm). He was used to check the gas tightness of the overall apparatus. Before starting the experiment, the adsorbent was regenerated with an inlet He flow of 100 mL/min at 473 K for 2 h. The system adsorption pressure was then stabilized to 120 kPa with He

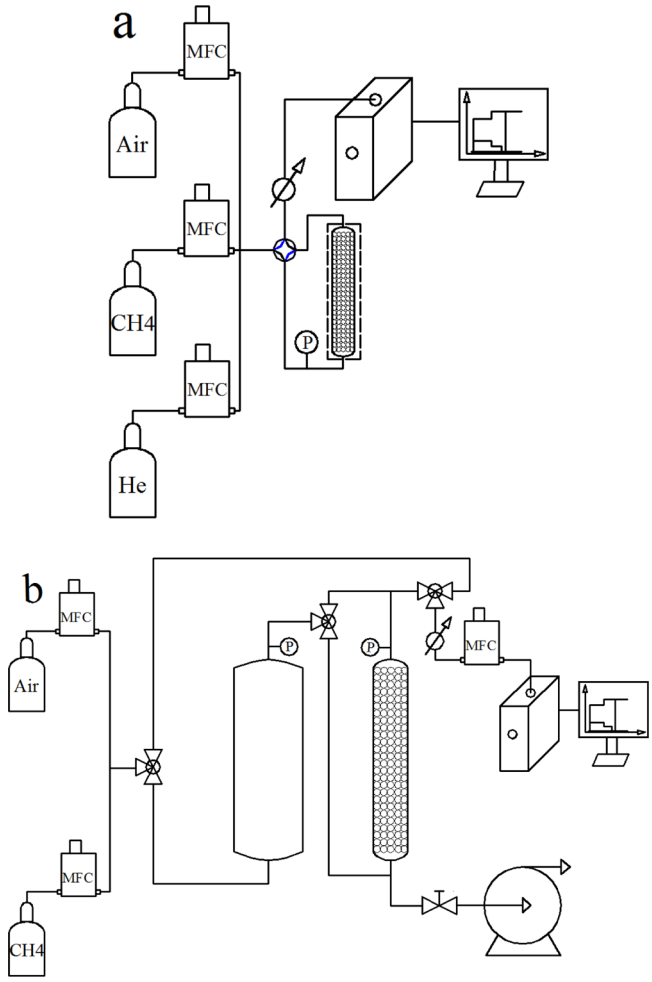

Figure 8. Schematic diagrams of $CH_4/O_2/N_2$ breakthrough experiment (a) and CH_4 enrichment experiment (b).

using a back-pressure valve. The breakthrough temperature was set to 308 K. Breakthrough tests were started by opening the valve between the mixture gas and the packed column. The components of the product gas were analyzed using the on-line mass spectrometer [Beishide Instrument Technology (Beijing) Co., Ltd.].

4.1.5. Enrichment Performance in Micro-positive Pressure VPSA. Practical enrichment performance of the $CH_4/O_2/N_2$ mixture without He was evaluated using an in-house-fabricated purification apparatus (micro-positive pressure VPSA), as shown in Figure 8b. First, the adsorbent (125.0 g) was placed in the adsorption bed (length: 60 cm, diameter: 2 cm) and the system vacuum was maintained at approximately −0.1 MPa. The mixture of $CH_4/O_2/N_2$ was then injected into the gasholder (length: 60 cm, diameter: 4 cm) until the pressure reached 140 kPa. The system adsorption pressure was stabilized to 120 kPa with the feed gas passing directly through the back-pressure valve in the bypass. A mass flow controller (MFC) was installed to record the amounts of outlet gas. The real-time concentrations of product gas components were detected using an on-line mass spectrometer. The product gases of different periods were collected and measured by gas chromatography (GC-9860-5CNJ, Nanjing Hope Analytical Equipment Co., Ltd.). The corresponding CH_4 recovery was then calculated. Furthermore, the effect of O_2

https://dx.doi.org/10.1021/acsomega.0c06148
ACS Omega 2021, 6, 6914−6923

removal and methane enrichment was evaluated from the analysis results.

4.2. Mathematical Models. *4.2.1. Adsorption Equilibrium.* Langmuir and Sips models were used for fitting the adsorption isotherms in this work. The relationship between the heterogeneous surface of an adsorbent and the adsorption equilibrium process was investigated.

The Langmuir model,[49] which assumes that the adsorbate on the sorbent is a monolayer and the surface of the sorbent is homogeneous, is the most commonly used model for adsorption isotherm fitting. The model is described by the following equation

$$q = \frac{q_m bp}{1 + bp} \tag{1}$$

According to previous studies, the heterogeneity factor (n) is a critical parameter in adsorption equilibrium due to the heterogeneous surface of most adsorbents. The Sips model[29] was employed to fit adsorption isotherms, where the n value is considered. The model is governed by the following equation

$$q = \frac{q_m (bp)^{1/n}}{1 + (bp)^{1/n}} \tag{2}$$

where q (mmol/g) is the adsorption amount at equilibrium pressure p (MPa), q_m (mmol/g) is the adsorptive saturation capacity, and b (MPa^{-1}) is the adsorption affinity constant, which indicates the adsorbed strength of an adsorbate attached to the CMS-3KT.

The deviation of the experimental data from the model was defined as the mean absolute percentage error (MAPE)

$$\mathrm{MAPE}(\%) = \frac{100}{j}\sum_{i=1}^{j}\left|\frac{q_{cal,i} - q_{exp,i}}{q_{exp,i}}\right| \tag{3}$$

where j, $q_{exp,i}$, and $q_{cal,i}$ denote the number of experimental data, experimental data, and data calculated by the isotherm models corresponding to $q_{exp,i}$, respectively.

4.2.2. Adsorption Heat. The adsorption isosteric heat affected the adsorption amounts of adsorbate on the sorbent and was therefore essential for the design of the adsorption bed used in gas enrichment.

In this work, the integral heat was measured by a C80 microcalorimeter and was related to the isosteric heat as follows[50]

$$q_{st} = \frac{dq_{exp}}{dn} \tag{4}$$

where q_{st} is the isosteric heat, q_{exp} is the integral heat, and n is the adsorption amount. q_{st} can be calculated as follows[49]

$$q_{st} = \frac{q_{exp,i+1} - q_{exp,i}}{n_{i+1} - n_i} = \frac{\Delta q_{exp,i}}{\Delta n} \tag{5}$$

where $q_{exp,i}$ is the integral heat at the equilibrium pressure p_i and q_{st} is the isosteric heat when the adsorption amount is equal to $(n_i + n_{i+1})/2$.

4.2.3. Adsorption Kinetics. The diffusivity is a critical parameter for predicting the kinetics-based separation possibility of a gas mixture. Therefore, the diffusivity of gas entering the adsorbent considered in this work was calculated using a micropore diffusion model. When the ratio of m_t and m_∞ ranges from 70% to 90%, the adsorption uptake curve can be related to the diffusion time constant (D_c/r_c^2) as follows[51]

$$1 - \frac{m_t}{m_\infty} \approx \frac{6}{\pi^2}\exp\left(\frac{-\pi^2 D_c t}{r_c^2}\right) \tag{6}$$

where m_t (mmol/g) is the adsorption amount at time t (s), m_∞ (mmol/g) is the adsorption amount at equilibrium, r_c is the adsorbent diameter, D_c is the effective diffusivity, and D_c/r_c^2 is the diffusion time constant.

The D_c/r_c^2 of each gas was estimated from the slope of a linear plot obtained for $\mathrm{Ln}(1 - (m_t/m_\infty))$ versus t at a specific pressure.

■ ASSOCIATED CONTENT

Supporting Information

The Supporting Information is available free of charge at https://pubs.acs.org/doi/10.1021/acsomega.0c06148.

Adsorption isotherms of CH_4, O_2, and N_2 in 313 and 318 K; adsorption amounts for CH_4, N_2, and O_2 on CMS-3KT in referenced studies; integral heats of adsorption for CH_4, O_2, and N_2 in 308, 313, and 318 K; and linear fitting of adsorption uptake curves for O_2, N_2, and CH_4 on CMS-3KT at 0.1 MPa in 308, 313, and 318 K (PDF)

■ AUTHOR INFORMATION

Corresponding Authors

Hong Liu − *Jiangsu Key Laboratory of Fire Safety in Urban Underground Space, China University of Mining and Technology (CUMT), Xuzhou 221116, PR China; National Engineering Research Centre for Coal Gas Control, China University of Mining and Technology (CUMT), Xuzhou 221116, PR China; Faculty of Safety Engineering, China University of Mining and Technology (CUMT), Xuzhou 221116, PR China;* orcid.org/0000-0001-6360-8134; Email: liuhong2013@cumt.edu.cn

Fubao Zhou − *Jiangsu Key Laboratory of Fire Safety in Urban Underground Space, China University of Mining and Technology (CUMT), Xuzhou 221116, PR China; National Engineering Research Centre for Coal Gas Control, China University of Mining and Technology (CUMT), Xuzhou 221116, PR China; Faculty of Safety Engineering, China University of Mining and Technology (CUMT), Xuzhou 221116, PR China;* orcid.org/0000-0002-9464-2252; Email: f.zhou@cumt.edu.cn

Authors

Jie Zhang − *Jiangsu Key Laboratory of Fire Safety in Urban Underground Space, China University of Mining and Technology (CUMT), Xuzhou 221116, PR China; Faculty of Safety Engineering, China University of Mining and Technology (CUMT), Xuzhou 221116, PR China*

Xingcheng Li − *Jiangsu Key Laboratory of Fire Safety in Urban Underground Space, China University of Mining and Technology (CUMT), Xuzhou 221116, PR China; Faculty of Safety Engineering, China University of Mining and Technology (CUMT), Xuzhou 221116, PR China*

Kangwei Wei − *Jiangsu Key Laboratory of Fire Safety in Urban Underground Space, China University of Mining and Technology (CUMT), Xuzhou 221116, PR China; Faculty of Safety Engineering, China University of Mining and Technology (CUMT), Xuzhou 221116, PR China*

https://dx.doi.org/10.1021/acsomega.0c06148
ACS Omega 2021, 6, 6914−6923

Jiaojiao Song − *Jiangsu Key Laboratory of Fire Safety in Urban Underground Space, China University of Mining and Technology (CUMT), Xuzhou 221116, PR China; Faculty of Safety Engineering, China University of Mining and Technology (CUMT), Xuzhou 221116, PR China*

Complete contact information is available at: https://pubs.acs.org/10.1021/acsomega.0c06148

Notes

The authors declare no competing financial interest.

■ ACKNOWLEDGMENTS

This research was supported by the Program for Changjiang Scholars and Innovative Research Team in University (IRT_17R103), the Fundamental Research Funds for the Central Universities (2018CXTD01), the 2nd Xplorer Prize sponsored by the Tencent Foundation, and A Project Funded by the Priority Academic Program Development of Jiangsu Higher Education Institutions (PAPD).

■ REFERENCES

(1) Mastalerz, M. Coal bed methane: reserves, production and future outlook. In *Future Energy*, 2nd ed.; Letcher, T. M., Ed.; Elsevier: Bloomington, 2014; pp. 145−158.
(2) Liu, X.; Xie, W.; Cui, X.; Tan, Z.; Cao, J.; Chen, Y. Clinoptilolite tailored to methane or nitrogen selectivity through different temperature treatment. *Chem. Phys. Lett.* **2018**, *707*, 75−79.
(3) Wang, J.; Mohr, S.; Feng, L.; Liu, H.; Tverberg, G. E. Analysis of resource potential for China's unconventional gas and forecast for its long-term production growth. *Energy Pol.* **2016**, *88*, 389−401.
(4) Su, S.; Agnew, J. Catalytic combustion of coal mine ventilation air methane. *Fuel* **2006**, *85*, 1201−1210.
(5) Moore, T. A. Coalbed methane: a review. *Int. J. Coal Geol.* **2012**, *101*, 36−81.
(6) Wang, L.; Liu, S.; Cheng, Y.; Yin, G.; Zhang, D.; Guo, P. Reservoir reconstruction technologies for coalbed methane recovery in deep and multiple seams. *Int. J. Min. Sci. Technol.* **2017**, *27*, 277−284.
(7) Karacan, C. Ö.; Ruiz, F. A.; Cotè, M.; Phipps, S. Coal mine methane: a review of capture and utilization practices with benefits to mining safety and to greenhouse gas reduction. *Int. J. Coal Geol.* **2011**, *86*, 121−156.
(8) Palmer, I. Coalbed methane completions: a world view. *Int. J. Coal Geol.* **2010**, *82*, 184−195.
(9) Bhadra, S. J.; Farooq, S. Separation of methane-nitrogen mixture by pressure swing adsorption for natural gas upgrading. *Ind. Eng. Chem. Res.* **2011**, *50*, 14030−14045.
(10) Cavenati, S.; Grande, C. A.; Rodrigues, A. E. Removal of carbon dioxide from natural gas by vacuum pressure swing adsorption. *Energy Fuels* **2006**, *20*, 2648−2659.
(11) Bertrand, D. Process for Removing Nitrogen from Natural Gas. U.S. Patent, 0,363,977 A1, 2018.
(12) Elkamel, A.; Noble, R. D. A statistical mechanics approach to the separation of methane and nitrogen using capillary condensation in a microporous membrane. *J. Membr. Sci.* **1992**, *65*, 163−172.
(13) Happel, J.; Hnatow, M. A.; Meyer, H. The study of separation nitrogen from methane by hydrate formation using a novel apparatus. *Ann. N.Y. Acad. Sci.* **1994**, *715*, 412−424.
(14) Saleman, T. L.; Li, G. K.; Rufford, T. E.; Stanwix, P. L.; Chan, K. I.; Huang, S. H.; May, E. F. Capture of low grade methane from nitrogen gas using dual-reflux pressure swing adsorption. *Chem. Eng. J.* **2015**, *281*, 739−748.
(15) Qu, D.; Yang, Y.; Lu, K.; Yang, L.; Li, P.; Yu, J.; Ribeiro, A. M.; Rodrigues, A. E. Microstructure effect of carbon materials on the low-concentration methane adsorption separation from its mixture with nitrogen. *Adsorption* **2018**, *24*, 357−369.
(16) Zhang, J.; Qu, S.; Li, L.; Wang, P.; Li, X.; Che, Y.; Li, X. Preparation of carbon molecular sieves used for CH4/N2 separation. *J. Chem. Eng. Data* **2018**, *63*, 1737−1744.
(17) Gu, M.; Zhang, B.; Qi, Z.; Liu, Z.; Duan, S.; Du, X.; Xian, X. Effects of pore structure of granular activated carbons on CH4 enrichment from CH4/N2 by vacuum pressure swing adsorption. *Sep. Purif. Technol.* **2015**, *146*, 213−218.
(18) Bae, Y.-S.; Moon, J.-H.; Ahn, H.; Lee, C.-H. Effects of adsorbate properties on adsorption mechanism in a carbon molecular sieve. *Korean J. Chem. Eng.* **2004**, *21*, 712−720.
(19) Bae, Y.-S.; Lee, C.-H. Sorption kinetics of eight gases on a carbon molecular sieve at elevated pressure. *Carbon* **2005**, *43*, 95−107.
(20) Li, Y. L.; Liu, Y. S.; Yang, X. Proportion pressure swing adsorption for low concentration coal mine methane enrichment. *Sep. Sci. Technol.* **2013**, *48*, 1201−1210.
(21) Yang, X.; Liu, Y.; Li, Y.; Meng, Y.; Zhang, C.; Yan, J. Safe separation of the low-concentration and oxygen-bearing coal mine methane by vacuum pressure swing adsorption. *Adsorpt. Sci. Technol.* **2014**, *32*, 667−679.
(22) Olajossy, A.; Gawdzik, A.; Budner, Z.; Dula, J. Methane separation from coal mine methane gas by vacuum pressure swing adsorption. *Chem. Eng. Res. Des.* **2003**, *81*, 474−482.
(23) Olajossy, A. Effective recovery of methane from coal mine methane gas by vacuum pressure swing adsorption: a pilot scale case study. *Chem. Eng. Sci.* **2013**, *1*, 46−54.
(24) Zhou, Y.; Fu, Q.; Shen, Y.; Sun, W.; Zhang, D.; Li, D.; Yan, H. Upgrade of low-concentration oxygen-bearing coal bed methane by a vacuum pressure swing adsorption process: performance study and safety analysis. *Energy Fuels* **2016**, *30*, 1496−1509.
(25) Yang, X.; Li, Z.; Zhang, C.; Wang, H.; Zhang, E.; Xing, Y.; Xiao, P.; Yang, R. T.; Liu, Y.; Webley, P. A. Practical separation performance evaluation of coal mine methane upgrading with carbon molecular sieves. *Chem. Eng. J.* **2019**, *367*, 295−303.
(26) Yang, R. T. *Gas Separation by Adsorption Processes*; Butterworth-Heinemann, 2013.
(27) Sing, K. S. W.; Everett, D. H.; Haul, R. A. W. Reporting physisorption data for gas/solid systems with special reference to the determination of surface area and porosity (Recommendations 1984). *Pure Appl. Chem.* **1985**, *57*, 603−619.
(28) Arcoya, A.; González, J. A.; Llabre, G.; Seoane, X. L.; Travieso, N. Role of the countercations on the molecular sieve properties of a clinoptilolite. *Microporous Mater.* **1996**, *7*, 1−13.
(29) Park, D.; Ju, Y.; Kim, J.-H.; Ahn, H.; Lee, C.-H. Equilibrium and kinetics of nitrous oxide, oxygen and nitrogen adsorption on activated carbon and carbon molecular sieve. *Sep. Purif. Technol.* **2019**, *223*, 63−80.
(30) Cavenati, S.; Grande, C.; Rodrigues, A. Separation of methane and nitrogen by adsorption on carbon molecular sieve. *Sep. Sci. Technol.* **2005**, *40*, 2721−2743.
(31) Park, Y.; Moon, D.-K.; Park, D.; Mofarahi, M.; Lee, C.-H. Adsorption equilibria and kinetics of CO2, CO, and N2 on carbon molecular sieve. *Sep. Purif. Technol.* **2019**, *212*, 952−964.
(32) O'koye, I. P.; Benham, M.; Thomas, K. M. Adsorption of gases and vapors on carbon molecular sieves. *Langmuir* **1997**, *13*, 4054−4059.
(33) Yang, Y.; Ribeiro, A. M.; Li, P.; Yu, J.-G.; Rodrigues, A. E. Adsorption equilibrium and kinetics of methane and nitrogen on carbon molecular sieve. *Ind. Eng. Chem. Res.* **2014**, *53*, 16840−16850.
(34) Yang, B.; Xu, E. L.; Li, M. Purification of coal mine methane on carbon molecular sieve by vacuum pressure swing adsorption. *Sep. Sci. Technol.* **2016**, *51*, 909−916.
(35) Do, D. D. *Adsorption Analysis: Equilibria and Kinetics: (with CD Containing Computer Matlab Programs)*; World Scientific, 1998.
(36) Chowdhury, S.; Mishra, R.; Saha, P.; Kushwaha, P. Adsorption thermodynamics, kinetics and isosteric heat of adsorption of malachite green onto chemically modified rice husk. *Desalination* **2011**, *265*, 159−168.

(37) Loughlin, K. F.; Hassan, M. M.; Fatehi, A. I.; Zahur, M. Rate and equilibrium sorption parameters for nitrogen and methane on carbon molecular sieve. *Gas Sep. Purif.* **1993**, *7*, 264−273.
(38) Fatehi, A. I.; Loughlin, K. F.; Hassan, M. M. Separation of methane-nitrogen mixtures by pressure swing adsorption using a carbon molecular sieve. *Gas Sep. Purif.* **1995**, *9*, 199−204.
(39) Park, Y.-J.; Lee, S.-J.; Moon, J.-H.; Choi, D.-K.; Lee, C.-H. Adsorption Equilibria of O2, N2, and Ar on Carbon Molecular Sieve and Zeolites 10X, 13X, and LiX. *J. Chem. Eng. Data* **2006**, *51*, 1001−1008.
(40) Shang, J.; Li, G.; Gu, Q.; Singh, R.; Xiao, P.; Liu, J. Z.; Webley, P. A. Temperature controlled invertible selectivity for adsorption of N2 and CH4 by molecular trapdoor chabazites. *Chem. Commun.* **2014**, *50*, 4544−4546.
(41) Yang, X.; Epiepang, F. E.; Liu, Y.; Yang, R. T. Heats of adsorption on mixed-cation LiNa-LSX: estimating SIII site occupancy by Li. *Chem. Eng. Sci.* **2018**, *178*, 194−198.
(42) Reid, C. R.; Thomas, K. M. Adsorption of gases on a carbon molecular sieve used for air separation: linear adsorptives as probes for kinetic selectivity. *Langmuir* **1999**, *15*, 3206−3218.
(43) Rutherford, S. W.; Do, D. D. Characterization of carbon molecular sieve 3A. *Langmuir* **2000**, *16*, 7245−7254.
(44) Guo, X.; Ren, J.; Xie, C.; Lin, J.; Li, Z. A comparison study on the deoxygenation of coal mine methane over coal gangue and coke under microwave heating conditions. *Energy Convers. Manage.* **2015**, *100*, 45−55.
(45) Zhou, F.-x.; Zhao, J.-t.; Zhang, L.; Wu, Z.-w.; Wang, J.-g.; Fang, Y.-t.; Qin, Z.-f. Catalytic deoxygenating characteristics of oxygen-bearing coal mine methane in the fluidized bed reactor. *J. Fuel Chem. Technol.* **2013**, *41*, 523−529.
(46) Richard, M.-A.; Bénard, P.; Chahine, R. Gas adsorption process in activated carbon over a wide temperature range above the critical point. Part 1: modified Dubinin-Astakhov model. *Adsorption* **2009**, *15*, 43−51.
(47) Zhou, L.; Zhou, Y.; Li, M.; Chen, P.; Wang, Y. Experimental and Modeling Study of the Adsorption of Supercritical Methane on a High Surface Activated Carbon†. *Langmuir* **2000**, *16*, 5955−5959.
(48) Li, H.; Li, G.; Kang, J.; Zhou, F.; Deng, J. Analytical model and experimental investigation of the adsorption thermodynamics of coalbed methane. *Adsorption* **2019**, *25*, 201−216.
(49) Ye, Z.; Chen, D.; Pan, Z.; Zhang, G.; Xia, Y.; Ding, X. An improved Langmuir model for evaluating methane adsorption capacity in shale under various pressures and temperatures. *J. Nat. Gas Sci. Eng.* **2016**, *31*, 658−680.
(50) Auroux, A. Calorimetry and Thermal Methods in Catalysis. *Springer Series in Materials Science*; Springer: Berlin, 2013; pp 30−32.
(51) Ruthven, D. M. *Principles and Adsorption and Adsorption Processes*; Willey Interscience: New York, 1984; pp 168.

https://dx.doi.org/10.1021/acsomega.0c06148
ACS Omega 2021, 6, 6914−6923